Progress In Electromagnetics Research M, Vol. 14, 71–83, 2010

ANALYSIS OF MICROWAVE CAVITY LOADED WITH LOSSY DIELECTRIC SLAB BY MEANS OF MODE MATCHING METHOD AND OPTIMIZATION OF LOAD LOCATION

O. Süle

Department of Electronic Engineering
Uludag University
Görükle, Bursa 16059, Turkey

S. Kent

Department of Electronics & Communication Engineering
Istanbul Technical University
Maslak, Istanbul 34469, Turkey

Abstract—An analysis is presented by means of a mode matching method for two microwave cavities of different sizes which are fed by a TE_{10} waveguide and loaded with lossy dielectric slab type material. The accuracy of the results obtained is presented together with a comparison of the results which are obtained by the HFSS numerical method. Optimization of the load location was performed in order to maximize the electrical field on the material. The principle of this optimization is based on finding the existence of the positions in which the reflection coefficient S_{11} is the lowest. When the feeding guide for the two different microwave cavities was at the centre of the resonator, the change in the reflection coefficient distribution was detected according to the different positions of the material in the oven, and then the lowest positions were found. The changes in the electric field in the detected positions were recorded.

Received 17 June 2010, Accepted 24 August 2010, Scheduled 31 August 2010
Corresponding author: S. Kent (kents@itu.edu.tr).

1. INTRODUCTION

Microwave heating is widely used in industry due to its advantages over conventional heating methods [1]. However, it is rather difficult to design an appropriate system according to the material which will be heated in spite of the present numerical methods, and very few studies have been carried out in this field [2–5].

The results found by means of the present numerical methods are related to checking the accuracy of the method rather than optimization.

The mode matching method has been widely used in a large number of applications of electromagnetism [6]. A considerable number of studies have been presented on finding the parameter S_{11} in an inhomogenously loaded microwave resonator. In the studies carried out, amplitudes of the reflection coefficient related to the frequency have been obtained for the structures examined [7–11].

The parameter S_{11} changes depending on a considerable number of parameters such as frequency, the dimensions of the resonator, the position of the feeding guide on the resonator, the dielectric permittivity, the geometry of the load, and the position and size of the load in the microwave resonator. In the literature sufficient searches for the parameter S_{11} have not been carried out, especially from the point of view of microwave heating.

In the studies of numerical and hybrid methods such as the finite difference time domain, finite element method, and mode matching, the changes in the parameter S_{11} in the structures examined have been presented in comparison with each other [12–16].

Differently in this work, the scattering parameter S_{11} has been obtained by changing the position of the material along the z axis while keeping stable the factors which affect the scattering parameter S_{11} in the resonator loaded with lossy slab type dielectric material, such as the frequency, the dimensions of the resonator, and the position of the feeding guide on the resonator. In this way, the change in the electric field has been found in the resonator at the lowest values of the reflection coefficient. At these points the efficiency of the microwave oven is at a maximum and loss power density on the material can be at a maximum too.

2. THEORETICAL BACKGROUND

Basically, we can divide the resonator into four basic parts as shown in Figure 1.

c_1 is the starting point of the feeding guide's x coordinate and c_2

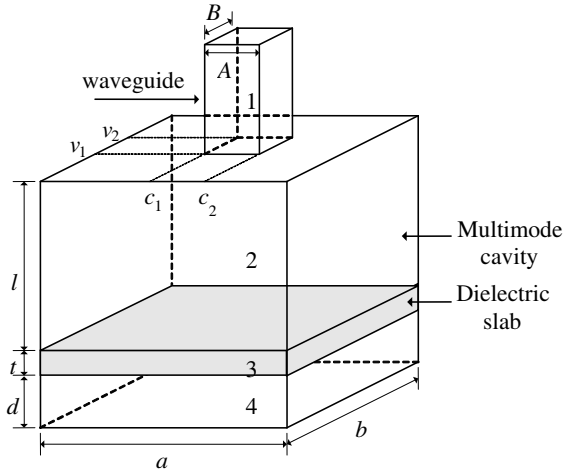

Figure 1. Three-dimensional rectangular cavity loaded with lossy slab.

is the last point of the feeding guide's x coordinate; in the same way v_1 is the starting point of the feeding guide's y coordinate and v_2 is the last point of the feeding guide's y coordinate. t is the slab thickness, d and l are the empty spaces of the resonator, and a and b are the resonator's x and y dimensions respectively.

When the basic equalities are taken into account and the equality of tangential electric field compounds (at the point of intersection of the first and the second area) on the aperture and mode matching equalities in the related boundaries (2) are used, the equation can be formulated as follows:

$$\vec{E}_s = \vec{e}^{\,h}_{t,10} e^{-jk_{z,10}z} \tag{1}$$

$$\vec{E}_t^I = \sum_{m=0}^{M}\sum_{n=0}^{N}\left[\begin{array}{l}\left(A^h_{mn}e^{+jk^I_{z,mn}z} + \delta_{mn,10}e^{-jk^I_{z,mn}z}\right)\vec{e}^{\,h(I)}_{t,mn} \\ +A^e_{mn}\vec{e}^{\,e(I)}_{t,mn}e^{+jk^I_{z,mn}z}\end{array}\right] \tag{2}$$

$$\vec{H}_t^I = \sum_{m=0}^{M}\sum_{n=0}^{N}\left[\begin{array}{l}\left(A^h_{mn}e^{+jk^{(I)I}_{z,mn}z} - \delta_{mn,10}e^{-jk^{(I)I}_{z,10}z}\right)\vec{h}^{\,h}_{t,mn} \\ +A^e_{mn}\,\vec{h}^{\,e}_{t,mn}e^{+jk^{(I)}_{z,mn}z}\end{array}\right] \tag{3}$$

$$\vec{E}_t^{II} = \sum_{m=0}^{M}\sum_{n=0}^{N}\left[\left(\begin{array}{l}B^{h(+)}_{mn}e^{-jk^{II}_{mn}z}\vec{e}^{\,h(II)}_{mn} \\ -B^{e(+)}_{mn}e^{-jk^{II}_{mn}z}\vec{e}^{\,e(II)}_{mn} \\ +B^{h(-)}_{mn}e^{jk^{II}_{mn}(z-l)}\vec{e}^{\,h(II)}_{mn} \\ +B^{e(-)}_{mn}e^{jk^{II}_{mn}(z-l)}\vec{e}^{\,e(II)}_{mn}\end{array}\right)\right] \tag{4}$$

$$\vec{H}_t^{II} = \sum_{m=0}^{M}\sum_{n=0}^{N}\left[\begin{pmatrix} -B_{mn}^{h(+)}e^{-jk_{mn}^{II}z}\vec{h}_{mn}^{h(II)} \\ +B_{mn}^{e(+)}e^{-jk_{mn}^{II}z}\vec{h}_{mn}^{e(II)} \\ +B_{mn}^{h(-)}e^{jk_{mn}^{II}(z-l)}\vec{h}_{mn}^{h(II)} \\ +B_{mn}^{e(-)}e^{jk_{mn}^{II}(z-l)}\vec{h}_{mn}^{e(II)} \end{pmatrix}\right] \tag{5}$$

$$k_{mn}^{I} = \sqrt{\omega^2\mu_o\varepsilon_0 - (m\pi/A)^2 - (n\pi/B)^2} \tag{6}$$

$$k_{mn}^{II} = \sqrt{\omega^2\mu_o\varepsilon_0 - (m\pi/a)^2 - (n\pi/b)^2} \tag{7}$$

where k is the mode propagation constant, e^h is the normal TE mode vector, h^h is the normal TM mode vector; m and n are mode indices, E_t is the tangential electric field, H_t is the tangential magnetic field.

For $z = 0 \vec{E}_t^{II} = \vec{E}_t^{I}$

$$(\delta_{mn,10}\vec{e}_{t,mn}^{h(I)} + A_{mn}^{h}\vec{e}_{t,mn}^{h(I)}) = \left(B_{mn}^{h(+)}\vec{e}_{mn}^{h(II)} + B_{mn}^{h(-)}e^{-j*k_{mn}^{II}l}\vec{e}_{mn}^{h(II)}\right) \tag{8}$$

$$(A_{mn}^{e}\vec{e}_{t,mn}^{e(I)}) = \left(-B_{mn}^{e(+)}\vec{e}_{mn}^{e(II)} + B_{mn}^{e(-)}e^{-j*k_{mn}^{II}l}\vec{e}_{mn}^{e(II)}\right) \tag{9}$$

In finding the reflection coefficient in the second part which is indicated with a minus sign, the equation below which consists of the effects of the third and fourth parts can be used as follows:

$$\Gamma_{23} = \frac{l_3 - Z_{er}}{l_3 + Z_{er}} \tag{10}$$

$$l_3 = Z_0\frac{e^{ik_{mn}^{II}d} - e^{-ik_{mn}^{II}d}}{e^{ik_{mn}^{II}d} + e^{-ik_{mn}^{II}d}} \tag{11}$$

$$\Gamma_{12} = \frac{l_2 - Z_0}{l_2 + Z_0} \tag{12}$$

$$l_2 = Z_{er}\frac{e^{\gamma t} + \Gamma_{23}e^{-\gamma t}}{e^{\gamma t} - \Gamma_{23}e^{-\gamma t}} \tag{13}$$

$$Z_{mn}^{h} = \frac{\omega\mu}{k_{mn}^{II}}, \quad Z_{mn}^{e} = \frac{k_{mn}^{II}}{\omega\varepsilon} \tag{14}$$

$$\gamma = \sqrt{(m\cdot\pi/a)^2 + (n\cdot\pi/b)^2 - \omega^2\mu_o\varepsilon_0\varepsilon_r} \tag{15}$$

$$B_{mn}^{-} = B_{mn}^{+}e^{-jk_{mn}^{II}l}\Gamma_{12} = B_{mn}^{+}\cdot\Gamma_0 \tag{16}$$

To enable the condition $z \times (\vec{H}_t^{II} - \vec{H}_t^{I}) = 0$ on the aperture ($z = 0$

plane)

$$\sum_{m=0}^{M}\sum_{n=0}^{N}\left[\begin{array}{l}\left(B_{mn}^{h(+)}\vec{e}_{mn}^{h(II)}\right)\left(\frac{1}{Z_{mn}^{h(II)}}+\frac{1}{Z_{mn}^{h(I)}}-\Gamma_0\cdot e^{-jk_{mn}^{II}l}\left(\frac{1}{Z_{mn}^{h(II)}}-\frac{1}{Z_{mn}^{h(I)}}\right)\right)-\\ \left(B_{mn}^{e(+)}\vec{e}_{mn}^{e(II)}\right)\left(\frac{1}{Z_{mn}^{e(II)}}+\frac{1}{Z_{mn}^{e(I)}}-\Gamma_0\cdot e^{-jk_{mn}^{II}l}\left(\frac{1}{Z_{mn}^{e(II)}}-\frac{1}{Z_{mn}^{e(I)}}\right)\right)\end{array}\right]$$
$$=2\delta_{10}\frac{1}{Z_{10}^{h(I)}}e_{10}^{h(I)} \tag{17}$$

We can write the approximate magnetic current as follows:

$$\left(\delta_{mn,10}+A_{mn}^{h}\right)=\int\limits_{S_a}\vec{M}_S\cdot\left(\hat{z}\times\vec{e}_{t,mn}^{h}\right)ds \tag{18}$$

$$A_{mn}^{e}=\int\limits_{S_a}\vec{M}_S\cdot\left(\hat{z}\times\vec{e}_{t,mn}^{e}\right)ds \tag{19}$$

$$B_{mn}^{h(+)}=\frac{1}{1+\Gamma_0\cdot e^{-jk_{mn}^{II}l}}\int\limits_{S_a}\vec{M}_S\cdot\left(\hat{z}\times\vec{e}_{t,mn}^{h}\right)ds \tag{20}$$

$$B_{mn}^{e(+)}=\frac{1}{-1+\Gamma_0\cdot e^{-jk_{mn}^{II}l}}\int\limits_{S_a}\vec{M}_S\cdot\left(\hat{z}\times\vec{e}_{t,mn}^{e}\right)ds \tag{21}$$

The magnetic current is approximated with a truncated set of independent basis functions:

$$\bar{M}_S\left(\vec{\rho'}\right)\cong\sum_{p}^{P}\left[a_{p_x}u_{p_x}\left(\vec{\rho'}\right)\hat{x}+a_{p_y}u_{py}\left(\vec{\rho'}\right)\hat{y}\right] \tag{22}$$

$$\left(\delta_{mn,10}+A_{mn}^{h}\right)=\sum_{m=0}^{M}\sum_{n=0}^{N}\int_{S_a}\left(-a_{mnx}u_{mnx}e_{y,mn}^{h}+a_{mny}u_{mny}e_{x,mn}^{h}\right)ds \tag{23}$$

$$A_{mn}^{e}=\sum_{m=0}^{M}\sum_{n=0}^{N}\int_{S_a}\left(-a_{mnx}u_{mnx}e_{y,mn}^{e}+a_{mny}u_{mny}e_{x,mn}^{e}\right)ds \tag{24}$$

$$\begin{aligned}&B_{mn}^{h(+)}+B_{mn}^{h(-)}\cdot e^{-jk_{mn}^{II}l}\\ &=\sum_{m=0}^{M}\sum_{n=0}^{N}\int_{S_a}\left(-a_{mnx}u_{mnx}e_{y,mn}^{h}+a_{mny}u_{mny}e_{x,mn}^{h}\right)ds\\ &-B_{mn}^{e(+)}+B_{mn}^{e(-)}\cdot e^{-jk_{mn}^{II}l}\\ &=\sum_{m=0}^{M}\sum_{n=0}^{N}\int_{S_a}\left(-a_{mnx}u_{mnx}e_{y,mn}^{e}+a_{mny}u_{mny}e_{x,mn}^{e}\right)ds\end{aligned} \tag{25}$$

$$\begin{bmatrix} B_{mn}^{h(+)} \\ B_{mn}^{e(+)} \end{bmatrix} = \begin{bmatrix} 1+\Gamma_0 \cdot e^{-jk_{mn}^{II} l} & 0 \\ 0 & -1+\Gamma_0 \cdot e^{-jk_{mn}^{II} l} \end{bmatrix}^{-1}$$
$$\begin{bmatrix} -\int\limits_{S_a} u_{mnx} e_{y,mn}^{h} ds & \int\limits_{S_a} u_{mny} e_{x,mn}^{h} ds \\ -\int\limits_{S_a} u_{mnx} e_{y,mn}^{e} ds & \int\limits_{S_a} u_{mny} e_{x,mn}^{e} ds \end{bmatrix} \begin{bmatrix} a_{mnx} \\ a_{mny} \end{bmatrix} \tag{26}$$
$$\begin{bmatrix} \left(\frac{1}{Z_{mn}^{h(II)}} + \frac{1}{Z_{mn}^{h(I)}} - \Gamma_0 \cdot \right. \\ \left. e^{-jk_{mn}^{II} l}\left(\frac{1}{Z_{mn}^{h(II)}} - \frac{1}{Z_{mn}^{h(I)}}\right)\right) \int\limits_{S_a} w_{sx} \vec{e}_{mn}^{h(II)} ds & -\left(\frac{1}{Z_{mn}^{e(II)}} + \frac{1}{Z_{mn}^{e(I)}} - \Gamma_0 \cdot \right. \\ \left. e^{-jk_{mn}^{II} l}\left(\frac{1}{Z_{mn}^{e(II)}} - \frac{1}{Z_{mn}^{e(I)}}\right)\right) \int\limits_{S_a} w_{sy} \vec{e}_{mn}^{e(II)} ds \\ \left(\frac{1}{Z_{mn}^{h(II)}} + \frac{1}{Z_{mn}^{h(I)}} - \Gamma_0 \cdot \right. \\ \left. e^{-jk_{mn}^{II} l}\left(\frac{1}{Z_{mn}^{h(II)}} - \frac{1}{Z_{mn}^{h(I)}}\right)\right) \int\limits_{S_a} w_{sx} \vec{e}_{mn}^{h(II)} ds & -\left(\frac{1}{Z_{mn}^{e(II)}} + \frac{1}{Z_{mn}^{e(I)}} - \Gamma_0 \cdot \right. \\ \left. e^{-jk_{mn}^{II} d}\left(\frac{1}{Z_{mn}^{e(II)}} - \frac{1}{Z_{mn}^{e(I)}}\right)\right) \int\limits_{S_a} w_{sy} \vec{e}_{mn}^{e(II)} ds \end{bmatrix}$$
$$\begin{bmatrix} 1+\Gamma_0 \cdot e^{-jk_{mn}^{II} l} & 0 \\ 0 & -1+\Gamma_0 \cdot e^{-jk_{mn}^{II} l} \end{bmatrix}^{-1}$$
$$\begin{bmatrix} -\int\limits_{S_a} u_{mnx} e_{y,mn}^{h} ds & \int\limits_{S_a} u_{mny} e_{x,mn}^{h} ds \\ -\int\limits_{S_a} u_{mnx} e_{y,mn}^{e} ds & \int\limits_{S_a} u_{mny} e_{x,mn}^{e} ds \end{bmatrix} \begin{bmatrix} a_{mnx} \\ a_{mny} \end{bmatrix}$$
$$= \begin{bmatrix} \frac{2}{Z_{10}^{h(I)}} \int\limits_{S_a} w_{sx} \vec{e}_{x10}^{h(I)} ds \\ \frac{2}{Z_{10}^{h(I)}} \int\limits_{S_a} w_{sy} \vec{e}_{y10}^{h(I)} ds \end{bmatrix} \tag{27}$$

By solving the matrix equation above it is possible to find the coefficients a_{mnx} and a_{mny}. After that B coefficients can be obtained by means of (19).

On the condition that the waveguide is between c_1 and c_2 in the x direction and between v_1 and v_2 in the y direction, the base and weighting functions can be presented as follows [17]:

$$\begin{aligned} u_{mnx} &= \sin\left(\frac{p\pi(x-c_1)}{c}\right)\cos\left(\frac{q\pi(y-v_1)}{v}\right) \\ w_{sx} &= \cos\left(\frac{s\pi(x-c_1)}{c}\right)\sin\left(\frac{t\pi(y-v_1)}{v}\right) \\ u_{mny} &= \cos\left(\frac{p\pi(x-c_1)}{c}\right)\sin\left(\frac{q\pi(y-v_1)}{v}\right) \\ w_{sy} &= \sin\left(\frac{s\pi(x-c_1)}{c}\right)\cos\left(\frac{t\pi(y-v_1)}{v}\right) \end{aligned} \tag{28}$$

3. NUMERICAL RESULTS

Numerical results have been obtained for two different resonators, of which one is small and the other is bigger. Firstly the changes in the reflection coefficient have been obtained by using as the load a lossy material with a width of 20 mm and dielectric permittivity of 2.5–0.1j and using a resonator whose dimensions are 125 mm, 93 mm, and 117 mm in the x, y, and z directions respectively. The operating frequency is 2.45 GHz. The resonator with dimensions of $125 \times 93 \times 117$ mm was used for numerical analysis in this work because when the resonator is empty there are a lot of resonant modes around 2.45 GHz.

The comparison of the results of Ansoft HFSS and mode matching for $d = 20$ mm is presented in Fig. 2 (for a 2.15–2.45 GHz wide band interval and a 100 MHz frequency change). HFSS is a commercial 3D full-wave Finite Element Method (FEM) solver for electromagnetic structures developed by Ansoft Corporation. The acronym originally stood for high frequency structural simulator. It to computes the electrical behavior of high-frequency and high-speed components. It is one of the common and powerful applications used for antenna design, and the design of complex RF electronic circuit elements including filters, transmission lines, and packaging. The software becomes the industry-standard simulation tool for 3D full-wave electromagnetic field simulation. HFSS provides E- and H-fields, currents, S-parameters and near and far radiated field results. Intrinsic to the

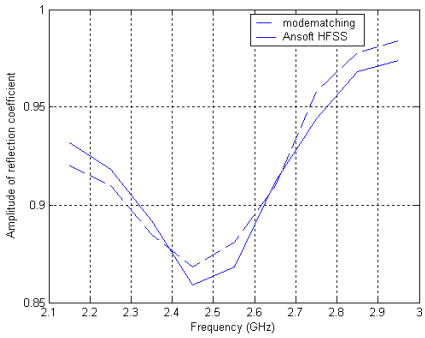

Figure 2. Reflection coefficient of the cavity as seen by the guide.

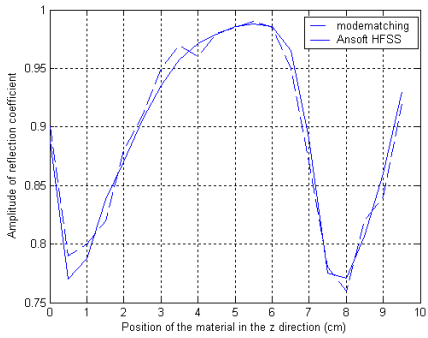

Figure 3. Amplitude of the reflection coefficient versus slab position obtained with mode matching and Ansoft HFSS at 2.45 GHz for the first cavity.

success of HFSS as an engineering design tool is its automated solution process where users are only required to specify geometry, material properties and the desired output. It generates an appropriate, efficient and accurate mesh for solving the problem using the proven finite element method. Ansoft HFSS is essential for field computations but it suffers with respect to the computational time and computer memory required to implement it.

Examining Fig. 3, it can be seen that the amplitude of the reflection coefficient is at the lowest point when the slab shaped load covering all the crosscuts is at $d = 0.5\,\text{cm}$ and at $d = 8\,\text{cm}$ and the amplitude of the reflection coefficient is at the highest point when the slab shaped load is at $d = 5.5\,\text{cm}$.

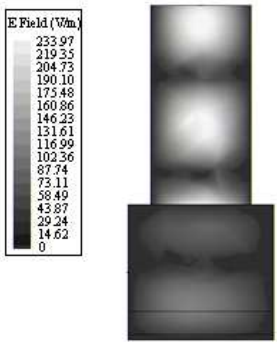

Figure 4. The change in the electric field in the resonator for $d = 0.5\,\text{cm}$.

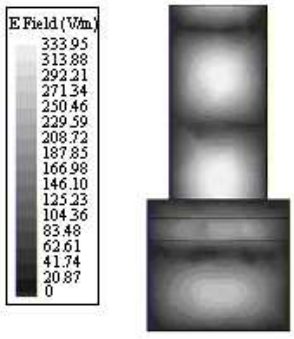

Figure 5. The change in the electric field in the resonator for $d = 8\,\text{cm}$.

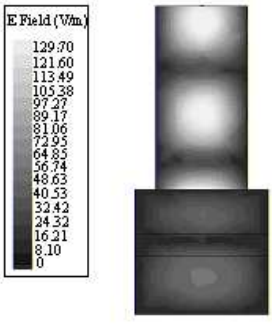

Figure 6. The change in the electric field in the resonator for $d = 5.5\,\text{cm}$.

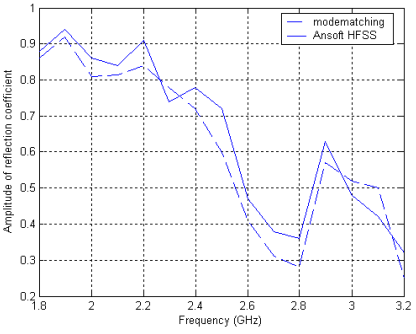

Figure 7. Comparison of the reflection coefficient amplitude.

When the positions of $d = 0.5\,\text{cm}$ and $d = 8\,\text{cm}$ are examined (Fig. 4 and Fig. 5, the points where the reflection coefficient is low) it can be said that the electrical field distribution on dielectric slab shaped material is more homogeneous and shows a wider distribution compared to the position of $d = 5.5\,\text{cm}$ (Fig. 6, the point where the reflection coefficient is high). This situation can be shown by means of (23), which has already expressed the power efficiency [2].

$$\eta = 1 - |S_{11}|^2 \tag{29}$$

The change in the reflection coefficient between 1.8 and 3.2 GHz has been presented for the second cavity in Fig. 7. The second cavity's dimensions are 37.8 cm, 25.8 cm, and 35.2 cm in the x, y, and z directions respectively. The slab shaped material's dielectric permittivity is 2.5–0.1j and it is placed at $d = 18\,\text{cm}$ and has a width of 2.6 cm. The feeding guide's x dimension is 8.6 cm, its y dimension is 4.3 cm, and it is placed entirely at the centre of the resonator.

The amplitudes of reflection coefficients have been drawn in these cases: 1) the waveguide is at the centre of the resonator; 2) the width of the material is 2.6 cm; and 3) the position of the material which is between the intervals of 8 and 23 cm of the resonator in the z direction has been changed every 0.5 cm.

It is clear from Fig. 8 that the amplitude of the reflection coefficient is at its lowest point at the height of $d = 11.5\,\text{cm}$. When the dielectric material is at the height of $d = 11.5\,\text{cm}$ and for the frequency band 2.3–2.6 GHz, which also includes the magnetron's

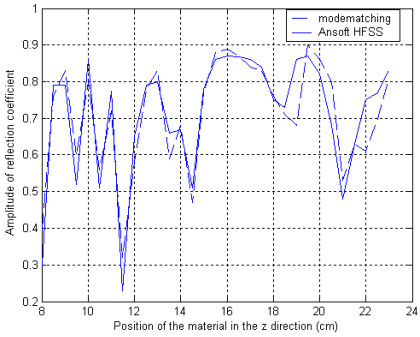

Figure 8. Amplitude of the reflection coefficient versus slab position obtained with mode matching and Ansoft HFSS at 2.45 GHz for the second cavity.

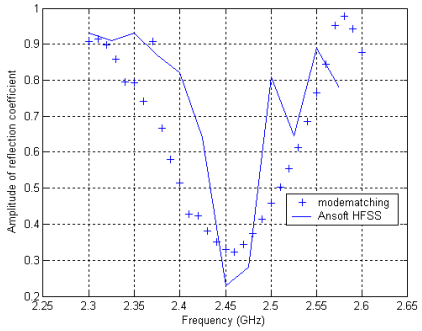

Figure 9. Comparison of the reflection coefficient amplitude.

operating frequency, 2.45 GHz, the position of the comparison of the Ansoft HFSS and mode matching methods is presented in Fig. 9.

It can be seen from Fig. 8 that the values of the position in which the reflection coefficient distribution is the lowest are at $d = 11.5$ cm, $d = 14.5$ cm, and $d = 21$ cm respectively. According to these positions electric field distributions have been found by means of Ansoft HFSS.

It can be seen from Figs. 10–13 that the electric field amplitude and power efficiency in the resonator are affected by the amplitude of the reflection coefficient. The electric field is distributed more efficiently in the resonator and on the dielectric material at the lowest point of reflection coefficient amplitudes.

Different analyses must be included for the different locations of the dielectric slab with Ansoft HFSS. In those analyses the reflection coefficient is obtained for a frequency interval which includes 2.45 GHz, whereas in this paper the frequency is determined as 2.45 GHz and the location of the dielectric slab is changed by chosen intervals in

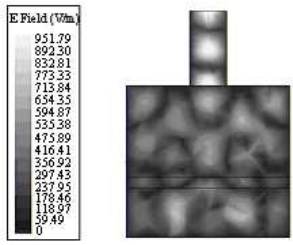

Figure 10. The electric field distribution in the resonator for $d = 11.5$ cm.

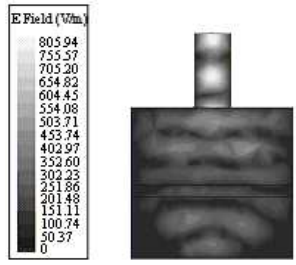

Figure 11. The electric field distribution in the resonator for $d = 14.5$ cm.

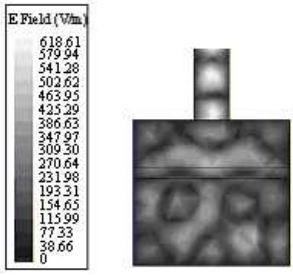

Figure 12. The electric field distribution in the resonator for $d = 21$ cm.

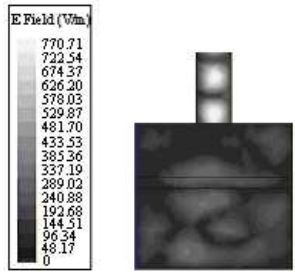

Figure 13. The electric field distribution in the resonator for $d = 19.5$ cm.

the Matlab program. In this way the reflection coefficient is obtained according to the location of the slab. By this process we can find the position which has the lowest reflection coefficient in a shorter time than when using Ansoft HFSS.

4. CONCLUSION

In this article, an analysis of a multimode resonator with the mode matching method has been presented. The changes in the amplitude of the reflection coefficient according to the frequency have been obtained and these results are compared to the results of Ansoft HFSS. By using this method, the positions of the material which will make the reflection coefficient the lowest in the microwave resonator have been found. The accuracy of the results has been presented in comparison with those obtained using Ansoft HFSS. The amplitudes of the reflection coefficients are obtained according to the slab shaped material in the z direction. In the microwave resonator, the changes in the electric field at the lowest reflection coefficient points have been found. The amplitudes of reflection coefficients have been examined for the position where the operating frequency and the position of the feeding guide are stable. It has been found that the reflection coefficient shows much variation in the dimensions of the resonator and the position of the material. The results achieved have been examined from the point of view of the electrical field distribution on the load, which directly affects microwave heating. In this way the efficiency of power in the multimode resonator has been maximized and also the appropriate values of the position of the material for microwave heating have been presented for the resonator.

Since the aim of this work is to present the accuracy of the method, the permittivity and loss of the dielectric material are not particularly chosen. Different materials which have different permittivities and losses can also be investigated by the same process.

A quasi linear change has been detected between the reflection coefficient change and the position of the load for the first oven, which is dimensionally smaller according to the feeding guide and which supports a smaller number of modes. Such a relationship as this has not been obtained for the second oven, which is dimensionally bigger and which supports a greater number of modes.

Optimization can be carried out for the stable operating frequency and feeding guide position on a specific resonator according to the position of load, as presented in this study. With the method presented in this article it is also possible to perform similar optimizations and to find the width of the load by keeping the feeding guide stable and

to find the position of the feeding guide by keeping the load position stable.

ACKNOWLEDGMENT

The authors would like to thank the three anonymous reviewers for their valuable contribution to improve the quality of this paper.

REFERENCES

1. Metaxas, A. C., "Radiofrequency and microwave heating: A perspective for the millennium," *Power Eng. J.*, Vol. 14, 51–60, 2000.
2. Requena-Perez, M. E., J. L. Pedreno-Molina, J. Monzo-Cabrera, and A. Diaz-Morcillo, "Multimode cavity efficiency optimizitation by optimum load location-experimental approach," *IEEE Trans. on Microwave Theory and Techn.*, Vol. 53, No. 6, 2144–2120, 2005.
3. Monzo-Cabrera, J., J. Escalante, A. Diaz Morcillo, A. Martinez-Gonzales, and D. Sanchez-Hernandez, "Load matching in multimode microwave-heating applicators based on the use of dielectric layer moulding with commercial material," *Microwave Opt. Technol. Lett.*, Vol. 41, 414–417, 2004.
4. Requena-Perez, M. E., J. L. Pedreno-Molina, M. Pinzolas-Prado, J. Monzo-Cabrera, A. Diaz-Morcillo, and D. Sanchez-Hernandez, "Load matching in multimode microwave-heating applicators by load location optimization," *Proc. 34th Eur. Microwave Conf.*, 1549–1552, 2004.
5. Walker, S. J., "Multi-mode cavity effects on the microwave heating of a ceramic slab," Ph.D. Thesis, The State University of New Jersey, 2001.
6. Jiang, Z. and Z. Shen, "Mode-matching analysis of large aperture coupling and its applications to the design of waveguide directional couplers," *IEEE Proc. — Microw. Antennas and Propag.*, Vol. 150, 422–428, 2003.
7. Setti, L. and S. Lefeuvre, "Model of a loaded 3D multimode cavity using a mixed method: 2D finite element method and modal analysis," *IEEE Transactions on Magnetics*, Vol. 31, 1574–1577, 1995.
8. Zhao, H., I. Turner, and F. W. Liu, "Numerical simulations of the power density distribution generated in a multimode cavity by using the method of lines technique to solve directly for the

electric field," *IEEE Trans. on Microwave Theory and Techn.*, Vol. 44, 2185–2194, 1996.

9. Mladenovic, M., A. Marincic, B. Milovanovic, and S. Ivkovic, "Identification of resonant modes in a loaded microwave rectangular cavity," *Journal of Microwave Power and Electromagnetic Energy*, Vol. 31, 30–34, 1998.
10. Dibben, D. C. and A. C. Metaxas, "Time domain finite element analysis of multimode microwave applicators loaded with low and high loss materials," *IEEE Microwave and Guided Letters*, Vol. 32, 945–948, 1996.
11. Jiang, Z. and Z. Shen, "Full wave analysis of cross-aperture waveguide couplers," *IEEE Microwave and Wireless Components Letters*, Vol. 12, 267–269, 2002.
12. Marocco, G. and F. Bardati, "Combined time and frequency domain modeling of electromagnetic radiation from apertures on resonant cavities by FDTD-MOM method," *Journal of Electromagnetic Waves and Applications*, Vol. 16, 523–539, 2002.
13. Zhao, H. I. and I. W. Turner, "An analysis of the finite-difference time-domain method for modeling the microwave heating of dielectric materials within a three-dimensional cavity system," *Journal of Microwave Power and Electromagnetic Energy*, Vol. 31, 199–214, 1996.
14. Liu, F., I. Turner, and M. E. Bialkowski, "A finite-difference time-domain simulation of power density distribution in a dielectric loaded microwave cavity," *J. Microwave power and Electromag. Energy*, Vol. 29, 138–148, 1994.
15. Bardi, I., O. Biro, K. Preis, G. Vrisk, and K. R. Richter, "Nodal and edge element analysis of inhomogeneously loaded 3D cavities," *IEEE Trans. on Microwave Theory and Techn.*, Vol. 28, 1142–1145, 1992.
16. Hallac, A. and A. C. Metaxas, "Finite element time domain analysis of microwave heating applicators using higher order vector finite elements," *Proc. 9th International Conference on Microwave and High Frequency Heating*, No. 21, UK, Sep. 2003.
17. Terril, N. D., "Field simulation for the microwave heating of thin ceramic fibers," MSc. Thesis, Virginia Pollytechnique Institute and State University, 1998.